The Landscape Fire Scars Database: mapping historical burned area and fire severity in Chile

Alejandro Miranda[1,2], Rayén Mentler[1], Ítalo Moletto-Lobos[3], Gabriela Alfaro[4], Leonardo Aliaga[1], Dana Balbontín[1], Maximiliano Barraza[1], Susanne Baumbach[1], Patricio Calderón[1], Fernando Cárdenas[1], Iván Castillo[1], Gonzalo Contreras[1], Felipe de la Barra[4], Mauricio Galleguillos[1,5], Mauro E. González[1,6,7], Carlos Hormazábal[1], Antonio Lara[1,6,8], Ian Mancilla[1], Francisca Muñoz[1], Cristian Oyarce[1], Francisca Pantoja[1], Rocío Ramírez[1] and Vicente Urrutia[1]

[1]Center for Climate and Resilience Research (CR)2, Santiago, Chile.

[2]Laboratorio de Ecología del Paisaje y Conservación, Departamento de Ciencias Forestales, Universidad de La Frontera, Temuco, Chile.

[3]Image Processing Laboratory, Global Change Unit, University of Valencia, Valencia, Spain.

[4]Industrial Engineering Department, University of Chile, Santiago, Chile.

[5] Facultad de Ingeniería y Ciencias, Universidad Adolfo Ibañez, Santiago, Chile.

[6]Instituto de Conservación, Biodiversidad y Territorio, Facultad de Ciencias Forestales y Recursos Naturales, Universidad Austral de Chile, Valdivia, Chile.

[7]Center for Fire and Socioecosystem Resilience (FireSES), Universidad Austral de Chile, Valdivia, Chile

[8]Fundación Centro de los Bosques Nativos FORECOS, Valdivia, Chile

Correspondence to: Alejandro Miranda (alejandro.miranda@ufrontera.cl)

Abstract. Achieving a local understanding of fire regimes requires high resolution, systematic and dynamic databases. High-quality information can help to transform the evidence into decision-making in the context of rapidly changing landscapes, particularly considering that geographical and temporal patterns of fire regimes and their trends vary locally over time. Global fire scar products at low spatial resolutions are available, but high-resolution wildfire data, especially for developing countries, is still lacking. Taking advantage of the Google Earth Engine (GEE) big-data analysis platform, we developed a flexible workflow to reconstruct individual burned areas and derive fire severity estimates for all reported fires. We tested our approach for historical wildfires in Chile. The result is the Landscape Fire Scars Database, a detailed and dynamic database that reconstructs 8,153 fires scars, representing 66.6% of the country's officially recorded fires between 1985 and 2018. For each fire event the database contains the following information: (i) Landsat mosaic of pre- and post-fire images; (ii) the fire scar in binary format; (iii) the remotely sensed estimated fire indexes (NBR, RdNBR), plus two vector files indicating (iv) the fire scar perimeter and (v) the fire scar severity reclassification. The Landscape Fire Scars Database for Chile and GEE script (JavaScript) are publicly available. The framework developed for the database can be applied anywhere in the world, the only requirement being its adaptation to local factors such as data availability, fire regimes, land cover or land cover dynamics, vegetation recovery, and cloud cover.

1 Introduction

Wildfires as a natural phenomenon have been a key component of the terrestrial system for millions of years, shaping biome structure and composition, and influencing the Earth's system cycles. Human activity has dramatically modified natural wildfire regimes and is now the main driver of their spatial and temporal patterns (Balch et al., 2017; Bowman et al., 2011). The changing fire regime has become an increasing threat to biodiversity (Kelly et al., 2020), agricultural and timber production (Stougiannidou et al., 2020; de la Barrera et al., 2018) and rural/peri-urban communities (Radeloff et al., 2018) as well as a major contributor to greenhouse gas emissions (Giglio et al., 2013). Recent estimates point to a global mean burned area of 337 to 423 Mha every year (Giglio et al., 2013, 2018). However, the geographical and temporal patterns of fire regimes and their trends over time vary locally depending on the source of ignition (Ganteaume and Syphard, 2018), climate characteristics and their changes (Jolly et al., 2015; Duane et al., 2021), predominant land use and land cover (Butsic et al., 2015), railroad density (Amato et al., 2018) as well as firefighting and fire suppression and prevention capacity (Bowman et al., 2011; Moritz et al., 2014). Additionally, each natural or anthropogenic forcing factor differs in its impact on fire regime attributes (e.g., ignition, severity, burned area, intensity) across multiple spatial and temporal scales worldwide (Ager et al., 2014; Balch et al., 2017; Fusco et al., 2016). An understanding of fire regimes at a local level requires high resolution, systematic and dynamic databases in order to transform the evidence into decision-making in these rapidly changing landscapes (Bowman et al., 2020).

Remote sensing provides pre-, during, and post-fire biophysical information necessary for conducting fire-risk assessment, fire detection and monitoring, assessment of fire impacts, and follow-up of changes in land cover trends after fire occurrence (Szpakowski and Jensen, 2019). Recent public datasets and products have enabled a better understanding of global and regional wildfire patterns (Giglio et al., 2016, 2018; Schroeder et al., 2014; Lizundia-Loiola et al., 2021). Although the principal active fire and burned area products contain information going back to the year 2000 (e.g., MODIS) with a spatial resolution in the best cases of more than 250 m (Chuvieco et al., 2018), there is still a lack of high-resolution wildfire data, especially for developing countries (Chuvieco et al., 2019). Andela et al. (2019) created a global dataset for the period 2003 to 2016 that estimates the size, duration, and propagation rate of individual wildfires with a spatial resolution of 500 m using MODIS products. Likewise, Artés et al., (2019), also using MODIS products, developed a global dataset to analyze fire regimes and fire behavior based on ignition dates and daily burned areas for individual wildfires. The large discrepancies between local and global estimates of burned area occur mostly in the case of fires of less than 100 ha due to detection difficulties when using coarse-resolution products (Roteta et al., 2019). This constitutes a significant barrier to the proper understanding of local wildfire regimes, and highlights the need for a high-resolution wildfire database (Chuvieco et al., 2019). Recent efforts using Landsat images have led to the identification of annual burn probabilities per pixel from which a database with a 30 m spatial resolution has been constructed that reaches back to the 1980s, but this has been done only for developed countries such as the USA and Australia (Goodwin and Collett, 2014; Hawbaker et al., 2017). However, recent

computational advances and the free availability of satellite imagery catalogs provide a promising framework for mapping annual burned areas worldwide at a spatial resolution of 30 m, which would be a major step forward in high-resolution wildfire database generation (Long et al., 2019).

In the case of Chile, the fire regime has been described mainly on the basis of the public wildfire database maintained by the Chilean Forest Service (CONAF), and with MODIS monthly burned area data used only in the most recent studies (de la Barrera et al., 2018; McWethy et al., 2018). Evidence regarding burned areas and fire frequency is derived from data with spatial resolutions between 500 m and 5 km (Gómez-González et al., 2019; González et al., 2018). From these large-scale datasets it has been determined that fire frequency is closely related to human footprint zones such as cities or other densely human-populated areas (Gómez-González et al., 2019; McWethy et al., 2018), roads (Miranda et al., 2020) and agricultural or industrial forest plantation activities (Gómez-González et al., 2019; McWethy et al., 2018). However, burned area also strongly interacts with climatic conditions favorable to the spread of fires, especially warmer and dryer years associated with El Niño-Southern Oscillation, wet winters the year previous (Holz et al., 2017; Urrutia-Jalabert et al., 2018) and severe drought (González et al., 2018). Such conditions have been more prevalent/frequent in recent years, with increasing temperatures and a general reduction in precipitation reported for the area since 1980 and a prolonged megadrought since 2010 (Boisier et al., 2016; Garreaud et al., 2019). Fire ignition near human communities, favorable climatic conditions and a lack of landscape or fuel management lead to increased wildfire occurrence (Úbeda and Sarricolea, 2016). However, this large-scale understanding may still be insufficient, especially for local applications such as fire spread modeling, fire severity estimation, landscape planning and design, ecological impacts and ecosystem resilience, or national greenhouse gas emission estimation.

An excellent opportunity for developing countries to generate their own local and historical high-resolution databases of wildfire scars is provided by Google Earth Engine (GEE) (Long et al., 2019). GEE is an open cloud-computing platform for geospatial analysis that contains a public catalog of satellite images, topography, land covers and other environmental datasets (Gorelick et al., 2017). Taken advantage of this big-data analysis platform, we generate a detailed database of fire scars in Chile through the development of a flexible workflow, enabling us to reconstruct individual burned areas and fire severity information for all reported historical fires. The result is our Landscape Fire Scars Database for Chile, which along with the GEE script (JavaScript) used to generate it are publicly available at https://www.pangaea.de/tok/6dcc6e08241c5076ef6bff47bbe73014308d4881 and https://code.earthengine.google.com/554027d16823525d890ab2f6c45167d9 respectively. This framework could be implementable for any geographical area globally, requiring only that it be adapted to local conditions regarding seed data availability, fire regimes, land cover or land cover dynamics, vegetation recovery and cloud cover.

2 Data and methods

2.1 Study site

The approach we developed was applied to central and south-central Chile (29°S-43°5'S), a long stretch of territory encompassing ten of the country's administrative regions (~255,120 Km^2). Fire activity in Chile is concentrated in this area, where considerable changes in land use and land cover have been observed in recent decades (Miranda et al., 2017), associated with increased fire activity (González et al., 2018).

2.1 Data seeding

To construct our historical database of fire scars, we used a subset of the public wildfire database provided by Corporación Nacional Forestal (CONAF). This agency records and stores information on all fires (> 0.01 ha) regarding their location, date, causes, area affected by land use, date and time of first control and suppression of fire, among other variables. The georeferencing system used by CONAF until 2003 assigned each fire to the center of a 1x1 km alphanumeric grid, based on the subdivision of 1:50,000 scale maps of the Military Geographic Institute (IGM). After 2003, the location of each fire and estimation of their burned area began to be carried out with the help of a Global Positioning System (GPS). Given the image availability, quality and spatial resolution of the Landsat programs, we extracted data only for fires with a burned area of more than 10 ha between 1985 and 2018 (N: 13,603). The 10 ha cut-off threshold was chosen since those fires represent more than 93% of the burned area according to the CONAF official information for 1985-2018 period. In addition, small fires are usually confounded with agricultural burning, a traditional cultural practice done by Chilean farmers. The original CONAF point dataset is included in our database's.

2.2 Fire scar generation

Our database was generated using JavaScript programming. The detailed workflow of the script developed to create individual fire scars is shown in Figure 1. It consists of the following consecutive steps: (i) input data selection and identification; (ii) pre- and post-fire image elaboration; (iii) index, mask calculation, and vectorization; (iv) spatial and spectral filtering; and (v) output data generation and exporting. As noted earlier, we have made the GEE script available to all users as a tool that can be adapted to local conditions and used for permanent database updating. The code is available at https://code.earthengine.google.com/554027d16823525d890ab2f6c45167d9.

The input data in Step (i) must be in the form of point data with geographic coordinates representing the ignition point or a point within the burned area. The points must indicate the fire start date, the fire control date (fire spread ending date) and the estimated burned area. In the absence of the last two, we used the fire start date and a fixed burned area of 100 ha as seed values for the initial assessment. The inputted seed data are converted into a list to processed and extracted individual fire

scars. Around each input point, a circular buffer area is created as a function of the estimated burned area, the precise dimensions given by $Bufferradius = log(burnedarea) * 2000$. Buffer area is explained because we may have only the fire's ignition point as a spatial reference. Therefore, it is necessary to explore near this point to find the limits of the fire scar. This could be an interactive process depending on the burned area or the shape of the fire scar.

In Step (ii), two image collections (sets of images) are prepared for each wildfire, depending on the fire start date. We use the atmospherically corrected surface reflectance and orthorectified images from Landsat 5 "LANDSAT/LT05/C01/T1_SR" (1984-2013), 7 "LANDSAT/LE07/C01/T1_SR" (1999-) and 8 (2013-) "LANDSAT/LC08/C01/T1_SR", with one image collection for a pre-fire condition and another for a post-fire condition, all of which are available in GEE. To avoid conflicts in mathematical operations for pre- and post-image collection generation, the date in day/month/year format is converted to Unix time format representing the number of milliseconds that have elapsed since January 1970. Based on the fire start and control dates, the respective image searches for both pre-fire post-fire events are each conducted for a period of 100 days. If this proves insufficient to get at least one image, the period can be extended up to two years for a pre-fire event and six months for a post-fire event. Pixels of snow, clouds, and cloud shadows are excluded from each image on the basis of the pixel quality band provided by Landsat and used as a binary mask of good and bad quality of the surface reflectance. For each image collection, we applied either the *mosaic* or the *median* reducer function to get a unique image of the landscape conditions at moments as close as possible before and after a fire event. This can be done by sorting the image by its date, obtaining the closer good quality pixels. When *mosaic* reducer did not provide good quality pixels, we applied the median reducer instead. The median method for reducing image collections avoids extreme values by selecting the median value for each pixel.

With the final pre- and post-mosaic images thus obtained, in Step (iii) we calculated all of the spectral indices (Table 1) used to identify the burned and unburned areas. The most widely used burned area index is the Normalized Burned Ratio (NBR) and its multitemporal form, the Delta Normalized Burn Ratio (dNBR) (Lentile et al., 2006; Fassnacht et al., 2021). These indexes reduce detection errors caused by shadows, water bodies, agricultural or tree harvesting, flooding and snowmelt (Chuvieco et al., 2019; Long et al., 2019). Other burned-area indexes have been proposed and a combination of them may give the best results, but to discriminate between burned and unburned areas we opted for the Relative Delta Normalized Burn Ratio (RdNBR). This index has shown good results in Mediterranean areas (Miller and Thode, 2007).

Table 1: Description of spectral indexes and formulas used in the workflow.

Index	Abbreviation	Formula	Usage	Reference
Normalized Difference Vegetation Index	NDVI	$\frac{\rho NIR - \rho RED}{\rho NIR + \rho RED}$	Detects pre- and post-fire vegetation cover	(Rouse et al, 1974)
Normalized Burned Ratio	NBR	$\frac{\rho NIR - \rho SWIR2}{\rho NIR + \rho SWIR2}$	Detects burned areas	(Key and Benson, 1999)
Delta Normalized Burn Ratio	dNBR	$PreFireNBR - PostFireNBR$	Detects changes in NIR and SWIR bands to identify burned area and fire severity	(Key and Benson, 1999)
Relative Delta Normalized Burn Ratio	RdNBR	$\frac{PreFireNBR - PostFireNBR}{\sqrt{ABS(PreFireNBR)}}$	Normalization of changes by pre-fire vegetation condition	(Miller and Thode, 2007)

Step (iv) involved the selection of the RdNBR index value for each wildfire that best captures the burned area based on visual interpretation. This is an interactive process (fire by fire) based on visual assessment of the best RdNBR value that delimitates each individual fire scar. The raster mask of the burned area was converted to a vector format for spatial and spectral filtering (Figure 1). By vectorizing the initially identified burned patches, spatial and spectral information could be added to each one so that burned and unburned patches could be better distinguished using new criteria. This information included the mean NDVI both before and after the fire event, the Near Infrared (NIR) minimum value after the event, and each patch's calculated area. The information added to the initial burned area patches could help to filter misclassified areas as burned areas, thus reducing commission errors. We also calculated the NDVI in order to estimate several vegetation parameters based on the red and infrared spectral bands (Table 1). The NDVI can be used to represent both the current state of, and changes over time in, the composition, structure, and phenology of vegetation, as well as plant health and even burned vegetation. (Helman, 2018; Pettorelli et al., 2005). Spatial filtering begins by defining an initial search distance to the ignition point of 1 km, but it can be interactively defined or modified later. The biggest patch within that distance is then identified and a new distance from this patch is defined. Only the patches within this latter distance are considered. In this stage, polygons or patches that may cause commission errors are eliminated from the areas counted as burned in the preliminary mask. They may include (a) water bodies with a pre-fire mean NDVI of less than 0.1; (b) polygons or patches for which the pre-fire mean NDVI is less than 0.1 and therefore did not contain vegetation, and other filtering criteria similar to those proposed by Long et al., (2019). Each polygon or patch satisfies the filter criteria and has a minimum area of 0.3 ha is retained. The filter values can be changed to suit local conditions.

Finally, in Step (v), once the fire scar is delimited, the event's severity is calculated from the RdNBR in a continuous raster format and categorized based on the ranges proposed by Miller and Thode (2007) (Severity category: Unchanged_<69, Low 69–315, Moderate 316–640, High >=641). Our database also makes available the pre- and post-fire NBR index for each image. Each fire scar and its severity are exported in vector and raster format, together with the multispectral corrected Landsat images of pre- and post-fire events and the RdNBR index. The vector data contains information about the fire record, the calculated area and the spectral responses used for filtering. The output name of each vector and raster file is OBJECT (FireScar, Severity, ImgPre, ImgPost and RdNBR) +_ISO-REGION_ID +_u-THRESHOLD RdNBR VALUE +_START DATE, where ISO-REGION is the name of the administrative region based on the ISO 3166-2:CL norm, ID is the identification number of the evaluated fire, THRESHOLD VALUE is the numerical value of the RdNBR index used to separate burned and unburned areas. Finally, START DATE is the date used to find the first image previous to the fire, which in most cases will be the same as the fire start date in the day/month/year format (e.g., FireScar_CL-RM_ID1920451_u330_19990215). A detailed description of each variable and its format is included as supplementary material in the database metadata.

2.3 Fire scar evaluation

We compared our fire scars with those generated by CONAF for the 2015-2016, 2016-2017 and 2017-2018 fire seasons. and published in Brull (2018). The author elaborated a manual digitalization of the fire scar perimeters using secondary information such as pre- and post-fire Landsat satellite images, dNBR index, Visible Infrared Imaging Radiometer Suite (VIIRS) active fire data, and Sentinel 2 images for high-resolution interpretation. The fire perimeters were defined as the outer limit between the burned and unburned area in the landscape, but the unburned areas inside this perimeter were not discounted in the final fire scars. The author generated 194 fire scars, of which 78 coincided with those we reconstructed and were thus the ones used for making comparisons. The mean area of the 78 fire scars was 1,180 ha (min: 200, max: 12,250). In order to avoid confusion between fire events, the evaluation carried out for individual fires located at least 300 m from any other scar dating to the same season. The evaluation of the 78 fire scars itself was based on the index proposed by Singh et al. (2015) that compares two georeferenced polygons using the Closeness Index (D) as formulated in Eq. (1) below:

$$D(i,j) = \sqrt{\left(OverSegementation(i,j)\right)^2 + \left(UnderSegementation(i,j)\right)^2} \quad (1)$$

where i = reference polygon, j = segment polygon, OverSegmentation (i, j) = $1 - \frac{A_{\text{intersect}}(i,j)}{A_{reference}(i)}$, UnderSegmentation (i, j) = $1 - \frac{A_{\text{intersect}}(i,j)}{A_{segment}(j)}$, Aintersect (i, j) = common area between segment polygon j and corresponding reference polygon i, Areference (i) = Area of reference polygon i, and Asegment (j) = Area of segment polygon j

In order to normalize the values of D, we use the modification form $D_{norm} = 1 - \left(\frac{D}{\sqrt{(2)}}\right)$,

where D_{norm} is the normalization of D values between 0 (no matching polygons) and 1 (perfectly matching polygons).

To assess the accuracy of our framework we include the evaluation of commission and omission error calculated as follow; commission error = FP/(FP+TP) and omission error = FN/(FN+TP), where FP is the spatial explicit false positive area of the generated fire scar compared with reference polygon of Brull (2018), FN is the false negative area and TP is the true positive area.

2.4 Database quality control

Even though the data generation process is done with standard and stable GEE scripts, the project's enormous scope could lead to involuntary discordances in resulting files. A thorough revision was performed over approximately 140,000 files, taking into account three major areas: (i) file and layer naming, file readability and type and amount of files per fire scar; (ii) geographic locations and burned area related revision; and (iii) dates and season related revision. The approach was to define several tests regarding relations between the content and attributes of the files in each area, that the whole dataset should comply. The revision scripts were written in Python in the Google Colab environment, having direct access to the Google Drive files generated by the GEE process. The tests were written for our resulting database but are generic in most terms and assumptions and are available at https://github.com/cr2uchile/Quality_Control_FireScarCL. Some of these tests led to human revision of the fires, either regenerating them or removing them from the firescar database, and other tests led to automated fixes, like name change or attribute column and content changes in the vector files. The resulting database of 8153 fire scar complies with the following statements:

- All fires have a unique identifier and 17 related files: Two satellite composite raster tif images that cover a domain larger than the identified fire scar, that merge pre and a post images (ImgPreF ..tif, ImgPosF ..tif), three raster tif images with the shape of the fire scar that contains: zeroes where there is no fire scar identified and ones where there is (FireScar ..tif); zeroes where there is no fire scar identified and severity index values (from 1 to 3) to identify the severity where there is a fire scar (Severity ..tif) and the RdNBR value (float numbers) for the points where there is a fire scar (RdNBR ..tif). Finally two

vector Shapefile images that contain six files each (.shx, .shp, .dbf, .cpg, .fix, .prj) where one is the vectorized representation of (FireScar ..shp) and the other is the vectorized representation of (Severity ..shp) with polygon and attributes information.

- For each set of resulting fire scar files, the ISO-REGION_ID corresponds to the region assigned by original CONAF point dataset, and the START_DATE corresponds to the ignition point assigned by CONAF. This was preserved to better identify the resulting fire scars with the seed database.

- All raster tif image files have the same area type and coordinate system. All pre and post-fire tif images have eight readable bands.

- For each fire: the pre and a post-fire tif images have the same width and height dimensions and the exact geographic extent. Also, their domain contains the firescar's ignition point and the resulting raster fire scar tif images (FireScar ..tif, Severity ..tif, RdNBR ..tif). The FireScar and Severity vector shapefiles files have consistent values in their attribute tables, and the amount of polygons of the Severity vector image is equal or more than the amount of polygons of the FireScar vector image. The dates in the attributes tables have format YYYY-MM-DD and the texts have UTF-8 encoding. The original fire names with accented vowels and ñ, were replaced by the non-accented vowels and n, respectively.

3. Results

Using the data for all 12,250 fires recorded by CONAF between 1985 and 2018 with a burned area greater than 10 ha, we were able to reconstruct 8,153 fire scars, 66.56% of the total registered fires (Table 2, Figure 1). Suitable images were found for 35% of recorded fires for the period 1985-1994, 63% for 1995-2004, 82% for 2005-2014 and 93% for 2015-2018. The increasing trend evident in these percentages reflects how image availability has grown over time. Smaller numbers of suitable images were found for the country's southern regions (Los Ríos and Los Lagos), the wettest and coldest included in our study, where cloud cover is continuous for much of the year (Table 2).

Table 2: Regional and temporal distribution of fires and reconstructed fire scars. The administrative regions are those included in the study. The number of fires column indicates the total recorded by CONAF for which burned area was over 0.01 ha, Yes is the number of reconstructed fire scars contained in our database, and No is the number of fire scars in the database that could not be reconstructed due to the unavailability of satellite images.

Administrative region	Number of fires	Number of fires >10ha	Reconstructed fires scars > 10ha (%)	Total fire scars 1985-2018		1985-1994		1995-2004		2005-2014		2015-2018	
				Yes	No	Yes	No	Yes	No	Yes	No	Yes	No
Coquimbo	1863	238	60.92	145	93	27	51	40	24	38	17	40	1
Valparaíso	31857	1784	80.38	1434	350	400	160	352	40	425	140	257	10
Metropolitana	15337	1109	85.75	951	158	208	79	252	42	261	33	230	4
Ohiggins	8249	1221	85.09	1039	182	240	93	251	56	365	26	183	7
Maule	14475	1419	65.89	935	484	103	290	199	118	393	52	240	24
Ñuble and Bío-Bío	77704	3248	58.07	1886	1362	124	775	473	375	712	171	577	41

Araucanía	31306	2369	57.41	1360	1009	30	458	346	356	424	131	560	64
Los Ríos	3680	339	35.99	122	217	8	154	41	48	33	10	40	5
Los Lagos	8416	523	53.73	281	242	5	100	53	111	143	27	80	4
Total	**192,887**	**12,250**	**66.6**	**8,153**	**4,097**	**1,145**	**2,160**	**2,007**	**1,170**	**2,794**	**607**	**2,207**	**160**

The total number of fires >0.01 ha exhibits a positive linear relationship with the total number of fires > 10 ha also recorded by CONAF between 1985 and 2018 (R^2 = 0.86). The number of recorded fires >10 ha and the number of reconstructed fire scars per region exhibits the same positive linear relationship (R^2 = 0.92), indicating that the distribution of the reconstructed data is regionally representative (Table 2, Figure 2). However, the pattern of relationships between recorded fires and reconstructed fire scars for the different regions varies from period to period. For 1985-1994 the relationship was weak (R^2 = 0.1) but had strengthened by 1995-2004 (R^2 = 0.91), and again for 2005-2014 (R^2 = 0.93) and 2015-2018 (R^2 = 0.93). The definitive version of our database is ordered by region and fire season to facilitate exploration and analysis, revealing, for example, the high levels of fire activity areas near the coastal cities of Valparaíso and Concepción over the various decades (Figure 3).

For each of the 8,153 reconstructed fire scars, our database contains the following: (i) a Landsat mosaic of pre- and post-fire event images (.tif) with eight spectral bands: blue, green, red, NIR, SWIR1 and SWIR2, NDVI and NBR index (Figure 4); (ii) the raster of the fire scar in binary format (.tif), where 1 is the burned area and 0 the unburned area (Figure 4); and (iii) the RdNBR index, both in continuous values (.tif) and categorized by severity classification level, where 0 is unchanged, 1 is low severity, 2 is medium severity and 3 is high severity (Miller and Thode, 2007) (Figure 4). In addition, there are two vector files (.shp) containing (iv) the fire scar perimeter and (v) the fire scar severity classification (Miller and Thode, 2007). Layers of information are assigned to each individual burned patch indicating its size, detected fire start and control dates, and spectral data. NBR bands are available for each image to enable reassessment of the fire scar and its severity. A detailed description of each variable and its format may be found in the database metadata.

3.1 Fire scar evaluation

We evaluated the fire scars reconstructed using our approach by contrasting them with the 78 scars derived from the official CONAF data that were suitable for making comparisons. A perfect match could not, of course, be expected given the differences in the two methodologies. One particularly crucial difference is that CONAF's fire scar digitalization includes within the fire perimeter for each fire event patches that in fact were not burned. These patches constituted anywhere from 13.5% to 18.2% of the areas indicated as burned, depending on the fire season (Brull, 2018). Also, CONAF's digitalization was complemented by the agency's own fieldwork, which improved the detection of low severity fires or surface fire under

the canopy. Nevertheless, the global accuracy assessment derived from the Closeness Index and calculated as the mean of the individual D_{norm} result in a value of 0.79. Examples of the comparisons of our reconstructed fire scars with CONAF data reported by (Brull, 2018) are shown in Figure 4 in together with the respective D_{norm} index for each case. Finally, we found a commission error = 7% and an omission error = 28%.

3.2 Limitations and other observations regarding the Landscape Fire Scars Database

1. Our fire scar dataset does not represent all of the fires recorded in the 1985-2018 period.
2. The reconstructed fire scars are mainly concentrated in the last 20 years of that period, which may be related to the improvement over time in image availability.
3. Remotely sensed fire severity estimates the change in spectral response in the burned area and must be carefully treated in the analysis of the fires' ecological impact. Low severity or surface fire may be underestimated.
4. Due to the 16-day interval between Landsat images, one fire scar reconstructed from them may represent more than one fire event in neighboring areas experiencing multiple fires over that interval, especially in the case of originally independent fire events that may have merged. Some fire scars in the database may be duplicated if they merged with another fire due to their proximity in space and time. We include a notification in the database where this could have happened.
5. Commission errors may occur due to other land cover changes such as tree plantation clearcutting or harvesting on crops.
6. In certain cases, the inclusion of additional available images of pre- and post-fire events may help to improve the fire scars.

4. Data availability

The Landscape fire scars dataset for Chile can be downloaded from the PANGAEA repository at https://www.pangaea.de/tok/6dcc6e08241c5076ef6bff47bbe73014308d4881 (Miranda et al., 2022).

5. Discussion and conclusions

The creation of our Landscape Fire Scars Database for Chile makes publicly available for the first time a high-resolution individual burned area product for the country. The georeferenced database is a multi-institutional effort containing information on more than 8,000 fires events of more than 10 ha between 1984 and 2018. It contains data on fire scar area, perimeter, and severity, which is accessible to the general public for analyzing future changes, improvements and new evaluations. Furthermore, the methodology for generating these data was implemented in GEE so that others may replicate our approach or apply it to other countries or cases where no openly accessible datasets are available. Public institutions and

researchers can take advantage of this framework to generate long-term time series of fire scars for any years of interest or just for one particularly significant wildfire. The international community can replicate this workflow using national fire occurrence data with the minimum required information or with recently released data on ignition coordinates, date, and fire duration for more than 13 million individual fires worldwide that occurred between 2003 and 2016 (Andela et al., 2019). As a high-resolution fire scar database, it should be of much help in conducting accurate and systematic evaluations of underlying wildfire forces, impacts and recoveries, and delineating populations and biodiversity, public policy and informed territorial decision making and planning (Chuvieco et al., 2019; Long et al., 2019; Stenzel et al., 2019).

Creating this database based on information distributed over an extensive territory on a national scale using a single method presented diverse challenges as regards (i) historical image availability, (ii) land cover and land cover change dynamics, and (iii) temporal image resolution and image cloud cover. In what follows, each of these issues is discussed in turn.

(i) Historical image availability

GEE (https://earthengine.google.com) provides free online access to original and corrected Landsat program data and products. Users do not need to download the images, and the analysis and image modification is also online, powered by Google servers (Gorelick et al., 2017). Image availability in the Landsat program is rather uneven across countries, with those in the developing world generally less well represented in terms of historical records. Nevertheless, the continuity of the image time series improves noticeably as the time period in question approaches the present. In the case of Chile, this pattern of improvement is clearly evidenced in the fire scare generation success rates we obtained for time periods since the mid-eighties (1985-1994: 35%, 1995-2004: 63%, 2005-2014: 82%, 2015-2018: 93%), consistent with the availability of free-cloud pixels for the country (Figure 5). This tendency must be considered when determining the time periods for reconstructing a database for any specific region. For example, according to the Landsat Global Archive Consolidation updates (Wulder et al., 2016), availability and usable image quality are lower for southern hemisphere high latitude regions (Huang et al., 2010; Stillinger et al., 2019; Viale et al., 2019).

(ii) Land cover change dynamics

Almost 90% of wildfire ignitions and burned areas worldwide are human-caused (Ganteaume and Syphard, 2018). As a result, many of these fires impact the wildland-urban interface, urban and rural settlements and productive regions (e.g., agricultural lands, tree plantations). Zones with high rates of land-use or land-cover changes may present some difficulties in fire scar and severity mapping. Remotely sensed burn area indexes are based on the abrupt change in the pre-fire spectral band values following a fire event. For example, NBR uses the near-infrared (NIR) and short wave infrared (SWIR) bands as proxies of photosynthetic productivity and water content of vegetated areas (Lentile et al., 2006; van Wagtendonk et al.,

2004). Both parameters are affected by fire, so the greater is the temporal difference in the index, the greater was the event's severity. However, the spectral response of those bands may also be influenced by other factors. Forestry activity, especially tree plantation clearcutting, deforestation or harvesting on agricultural land, as well as the drying of annual grassland in the summer season, dried meadows, and the cultural practice of burning agricultural wastes may all act to confuse the spectral response for a given landscape, assimilating them to wildfire (Ghermandi et al., 2019). Another local consideration is the recovery rate of the vegetation. For example, in the tropics recovery is faster than in temperate areas, which could affect mapping of burned areas or fire intensity estimation depending on how much time has passed between fire occurrence and acquisition of a good quality satellite image (Chuvieco et al., 2019). Local topography may also complicate the process of distinguishing burned areas in mountain zones due to the increased presence of shadows, fog, or melting snow in cold or high-elevation areas (Huang et al., 2010; Stillinger et al., 2019; Viale et al., 2019). Therefore, local experience in landscape dynamics and practice is crucial to ensuring the generation of accurate databases and may constitute a basis for adapting the most commonly used burned area indexes to local realities.

(iii) Temporal image resolution and image cloud cover

Landsat images are widely used to study land cover changes and trends thanks to their spatial and temporal resolution (Soulard et al., 2016). However, the 16-day interval between images could be a major limitation. In regions with high fire activity, this can make it more difficult to identify individual fire scars and differentiate them from those produced on other days at neighboring locations. This means that a single final fire scar may in fact have been created by multiple fire events occurring over the 16 days that converged or totally fused. The problem could be mitigated by using Sentinel-2 images (also available in GEE) for the earliest fire events given that the Sentinel-2 program is available from middle 2015 with a temporal resolution of 5-6 days (starting in 2017) and a pixel size of 10 m and 20 m (e.g. SWIR band), although increasing spatial resolution may raise another issue in that it could result in underestimation of the influence of dead vegetation shadows on the spectral index signals (Fassnacht et al., 2021). The high temporal resolution could also be helpful in zones with high cloud cover such as are found in tropical and high latitude or mountain areas (King et al., 2013). For example, we can observe that the Landsat archive in Africa could reduce its number of images with less than 40% of cloud cover in a mean of more than 25% with much fewer images in the tropical zone of the Congo Basin (Roy et al., 2010).

The RdNBR index is able to differentiate burned area over a diverse range of climate and geographic conditions. No evident pattern associated with the latitudinal or vegetation-type change was observed in applying the threshold value to identify scars. Different burned-land covers may have variable RdNBR values, but this relationship does not figure among the objectives for the present database development. In general, RdNBR performs wells when compared with field plots of severity. It is little influenced by the type of forest and is determined mainly by the fraction of consumed canopy cover (Cardil et al., 2019; Soverel et al., 2010; Fassnacht et al., 2021), demonstrating the index's high versatility. Nevertheless, the

task of assessing the performance of the severity classification is left to users of the database, and will depend on the local land cover context and field validations for identification of the best index. Our database does provide the NBR band for the images to facilitate comparison and evaluation of the dNBR and RdNBR indices.

The importance of the proposed database also stems from its value as a source of input for methods based on artificial intelligence (AI) aimed at automating the process of generating new fire scars. AI techniques such as machine learning (ML), deep learning (DL), and especially the convolutional neural network (CNN) are increasingly being used for classification or object segmentation problems (Alzubaidi et al., 2021). The integration of such methods with remote sensing data is enabling the development of burned area detection models that use human-delimited wildfire perimeters as their training data set. Promising results have been achieved using uni- or multi-temporal images and different types of remote sensing data to address the many open challenges in wildfire mapping and monitoring (Hu et al., 2021; Knopp et al., 2020; Pinto et al., 2021).

In conclusion, this present study makes, we believe, a significant contribution to the development of high-resolution methods for mapping fire scars and their temporal and spatial patterns. Our hope is that it will serve as a first step in an ongoing effort to build and maintain an extensive, consistent database on forest fires in Chile that will drive scientific research and improvements in landscape management. Further study is needed to broaden the current state of knowledge on local conditions through standardized field surveys.

(iv) Seeding datasets

Studies in Chile have previously evaluated the performance of the global satellite burned area products showing good performance. An improvement of thats products can be done using as seed point the fires detected by global datasets in Chile or another area. Global datasets such as MODIS Collection 6 burned area data MCD64A1 (Giglio et al., 2009), FIRMS (Schroeder, Wilfrid and Giglio, Louis, 2018) and Global Fire Atlas (Andela et al., 2019; Giglio et al., 2018) can be used for evaluating the performance of our approach in medium and large fires and create new high-resolution datasets for mapping fire scars in different ecosystems and land covers.

6. Acknowledgements

A.M., AL, MG, MGC, FM thank ANID/FONDAP/15110009, A.M. thanks the Agencia Nacional de Investigación y Desarrollo de Chile (ANID) Postdoctoral Fondecyt project 3210101 and FONDEF-IDEA ID20I10137. We also thank the support from the Complex Engineering Systems Institute PIA/BASAL AFB180003. M.E.G. thanks ANID/Fondecyt N° 1201528 and the Center for Fire and Socioecosistem Resilience (FireSES). The authors thank the Corporación Nacional Forestal (CONAF) for providing the seeding and digitalized fire scars data for database evaluation. Special acknowledgments to Jordi Brull and the hundreds of anonymous firefighters and professionals who have observed, surveyed, and developed the CONAF official fire records since 1984. We also thanks to the Chilean Institute for Disaster Resilience (ITREND) for their support.

Author contributions. A.M., R.M., I.M., M.E.G., A.L., I.C., M.G., designed the study, database and found acquisition. A.M. and R.M. managed the project and wrote the original draft with contributions from all other authors. A.M, R.M., G.A., L.A, D.B., M.B., S.B., P.C., F.C., G.C., F. dlB., C.H, I.M., C.O., F.P., R.R. and V. U. made the image interpretation, data processing, development of data bases, and providing different input on the manuscript and the database. F.M. made the data curation and database quality control.

Competing interests. The authors declare that they have no conflict of interest.

7. References

Ager, A. A., Preisler, H. K., Arca, B., Spano, D., and Salis, M.: Wildfire risk estimation in the Mediterranean area: MEDITERRANEAN WILDFIRE RISK ESTIMATION, Environmetrics, 25, 384–396, https://doi.org/10.1002/env.2269, 2014.

Alzubaidi, L., Zhang, J., Humaidi, A. J., Al-Dujaili, A., Duan, Y., Al-Shamma, O., Santamaría, J., Fadhel, M. A., Al-Amidie, M., and Farhan, L.: Review of deep learning: concepts, CNN architectures, challenges, applications, future directions, J. Big Data, 8, 53, https://doi.org/10.1186/s40537-021-00444-8, 2021.

Amato, F., Tonini, M., Murgante, B., and Kanevski, M.: Fuzzy definition of Rural Urban Interface: An application based on land use change scenarios in Portugal, Environ. Model. Softw., 104, 171–187, https://doi.org/10.1016/j.envsoft.2018.03.016, 2018.

Andela, N., Morton, D. C., Giglio, L., Paugam, R., Chen, Y., Hantson, S., van der Werf, G. R., and Randerson, J. T.: The Global Fire Atlas of individual fire size, duration, speed and direction, Earth Syst. Sci. Data, 11, 529–552, https://doi.org/10.5194/essd-11-529-2019, 2019.

Artés, T., Oom, D., de Rigo, D., Durrant, T. H., Maianti, P., Libertà, G., and San-Miguel-Ayanz, J.: A global wildfire dataset for the analysis of fire regimes and fire behaviour, Sci. Data, 6, 296, https://doi.org/10.1038/s41597-019-0312-2, 2019.

Balch, J. K., Bradley, B. A., Abatzoglou, J. T., Nagy, R. C., Fusco, E. J., and Mahood, A. L.: Human-started wildfires expand the fire niche across the United States, Proc. Natl. Acad. Sci., 114, 2946–2951, https://doi.org/10.1073/pnas.1617394114, 2017.

de la Barrera, F., Barraza, F., Favier, P., Ruiz, V., and Quense, J.: Megafires in Chile 2017: Monitoring multiscale environmental impacts of burned ecosystems, Sci. Total Environ., 637–638, 1526–1536, https://doi.org/10.1016/j.scitotenv.2018.05.119, 2018a.

de la Barrera, F., Barraza, F., Favier, P., Ruiz, V., and Quense, J.: Megafires in Chile 2017: Monitoring multiscale environmental impacts of burned ecosystems, Sci. Total Environ., 637–638, 1526–1536, https://doi.org/10.1016/j.scitotenv.2018.05.119, 2018b.

Boisier, J. P., Rondanelli, R., Garreaud, R. D., and Muñoz, F.: Anthropogenic and natural contributions to the Southeast Pacific precipitation decline and recent megadrought in central Chile, Geophys. Res. Lett., 43, 413–421, https://doi.org/10.1002/2015GL067265, 2016.

Bowman, D., Williamson, G., Yebra, M., Lizundia-Loiola, J., Pettinari, M. L., Shah, S., Bradstock, R., and Chuvieco, E.: Wildfires: Australia needs national monitoring agency, Nature, 584, 188–191, https://doi.org/10.1038/d41586-020-02306-4, 2020.

Bowman, D. M. J. S., Balch, J., Artaxo, P., Bond, W. J., Cochrane, M. A., D'Antonio, C. M., DeFries, R., Johnston, F. H., Keeley, J. E., Krawchuk, M. A., Kull, C. A., Mack, M., Moritz, M. A., Pyne, S., Roos, C. I., Scott, A. C., Sodhi, N. S., and Swetnam, T. W.: The human dimension of fire regimes on Earth: The human dimension of fire regimes on Earth, J. Biogeogr., 38, 2223–2236, https://doi.org/10.1111/j.1365-2699.2011.02595.x, 2011.

Brull, J. Análisis de la severidad de los incendios de magnitud de la temporada de incendios forestales 2017-2018, 2018. Corporación Nacional Forestal. Sección de Análisis y Predicción de Incendios Forestales. 38 p. Santiago, Chile.

Butsic, V., Kelly, M., and Moritz, M.: Land Use and Wildfire: A Review of Local Interactions and Teleconnections, Land, 4, 140–156, https://doi.org/10.3390/land4010140, 2015.

Cardil, A., Mola-Yudego, B., Blázquez-Casado, Á., and González-Olabarria, J. R.: Fire and burn severity assessment: Calibration of Relative Differenced Normalized Burn Ratio (RdNBR) with field data, J. Environ. Manage., 235, 342–349, https://doi.org/10.1016/j.jenvman.2019.01.077, 2019.

Chuvieco, E., Lizundia-Loiola, J., Pettinari, M. L., Ramo, R., Padilla, M., Tansey, K., Mouillot, F., Laurent, P., Storm, T., Heil, A., and Plummer, S.: Generation and analysis of a new global burned area product based on MODIS 250 m reflectance bands and thermal anomalies, Earth Syst. Sci. Data, 10, 2015–2031, https://doi.org/10.5194/essd-10-2015-2018, 2018.

Chuvieco, E., Mouillot, F., van der Werf, G. R., San Miguel, J., Tanase, M., Koutsias, N., García, M., Yebra, M., Padilla, M., Gitas, I., Heil, A., Hawbaker, T. J., and Giglio, L.: Historical background and current developments for mapping burned area from satellite Earth observation, Remote Sens. Environ., 225, 45–64, https://doi.org/10.1016/j.rse.2019.02.013, 2019.

Duane, A., Castellnou, M., and Brotons, L.: Towards a comprehensive look at global drivers of novel extreme wildfire events, Clim. Change, 165, 43, https://doi.org/10.1007/s10584-021-03066-4, 2021.

Edwards, E. J., Osborne, C. P., Stromberg, C. A. E., Smith, S. A., C4 Grasses Consortium, Bond, W. J., Christin, P. A., Cousins, A. B., Duvall, M. R., Fox, D. L., Freckleton, R. P., Ghannoum, O., Hartwell, J., Huang, Y., Janis, C. M., Keeley, J. E., Kellogg, E. A., Knapp, A. K., Leakey, A. D. B., Nelson, D. M., Saarela, J. M., Sage, R. F., Sala, O. E., Salamin, N., Still, C. J., and Tipple, B.: The Origins of C4 Grasslands: Integrating Evolutionary and Ecosystem Science, Science, 328, 587–591, https://doi.org/10.1126/science.1177216, 2010.

Fassnacht, F. E., Schmidt-Riese, E., Kattenborn, T., and Hernández, J.: Explaining Sentinel 2-based dNBR and RdNBR variability with reference data from the bird's eye (UAS) perspective, Int. J. Appl. Earth Obs. Geoinformation, 95, 102262, https://doi.org/10.1016/j.jag.2020.102262, 2021.

Fusco, E. J., Abatzoglou, J. T., Balch, J. K., Finn, J. T., and Bradley, B. A.: Quantifying the human influence on fire ignition across the western USA, Ecol. Appl., 26, 2390–2401, https://doi.org/10.1002/eap.1395, 2016.

Ganteaume, A. and Syphard, A. D.: Ignition Sources, in: Encyclopedia of Wildfires and Wildland-Urban Interface (WUI) Fires, edited by: Manzello, S. L., Springer International Publishing, Cham, 1–17, https://doi.org/10.1007/978-3-319-51727-8_43-1, 2018.

Garreaud, R. D., Boisier, J. P., Rondanelli, R., Montecinos, A., Sepúlveda, H. H., and Veloso-Aguila, D.: The Central Chile Mega Drought (2010–2018): A climate dynamics perspective, Int. J. Climatol., https://doi.org/10.1002/joc.6219, 2019.

Ghermandi, L., Lanorte, A., Oddi, F. J., and Lasaponara, R.: Assessing Fire Severity in Semiarid Environments with the DNBR and RDNBR Indices, Glob. J. Sci. Front. Res. H Environ. Earth Sci., 2019.

Giglio, L., Loboda, T., Roy, D. P., Quayle, B., and Justice, C. O.: An active-fire based burned area mapping algorithm for the MODIS sensor, Remote Sens. Environ., 113, 408–420, https://doi.org/10.1016/j.rse.2008.10.006, 2009.

Giglio, L., Randerson, J. T., and van der Werf, G. R.: Analysis of daily, monthly, and annual burned area using the fourth-generation global fire emissions database (GFED4): ANALYSIS OF BURNED AREA, J. Geophys. Res. Biogeosciences, 118, 317–328, https://doi.org/10.1002/jgrg.20042, 2013.

Giglio, L., Schroeder, W., and Justice, C. O.: The collection 6 MODIS active fire detection algorithm and fire products, Remote Sens. Environ., 178, 31–41, https://doi.org/10.1016/j.rse.2016.02.054, 2016.

Giglio, L., Boschetti, L., Roy, D. P., Humber, M. L., and Justice, C. O.: The Collection 6 MODIS burned area mapping algorithm and product, Remote Sens. Environ., 217, 72–85, https://doi.org/10.1016/j.rse.2018.08.005, 2018.

Gómez-González, S., González, M. E., Paula, S., Díaz-Hormazábal, I., Lara, A., and Delgado-Baquerizo, M.: Temperature and agriculture are largely associated with fire activity in Central Chile across different temporal periods, For. Ecol. Manag., 433, 535–543, https://doi.org/10.1016/j.foreco.2018.11.041, 2019.

González, M. E., Gómez-González, S., Lara, A., Garreaud, R., and Díaz-Hormazábal, I.: The 2010-2015 Megadrought and its influence on the fire regime in central and south-central Chile, Ecosphere, 9, e02300, https://doi.org/10.1002/ecs2.2300, 2018.

Goodwin, N. R. and Collett, L. J.: Development of an automated method for mapping fire history captured in Landsat TM and ETM+ time series across Queensland, Australia, Remote Sens. Environ., 148, 206–221, https://doi.org/10.1016/j.rse.2014.03.021, 2014.

Gorelick, N., Hancher, M., Dixon, M., Ilyushchenko, S., Thau, D., and Moore, R.: Google Earth Engine: Planetary-scale geospatial analysis for everyone, Remote Sens. Environ., 202, 18–27, https://doi.org/10.1016/j.rse.2017.06.031, 2017.

Hawbaker, T. J., Vanderhoof, M. K., Beal, Y.-J., Takacs, J. D., Schmidt, G. L., Falgout, J. T., Williams, B., Fairaux, N. M., Caldwell, M. K., Picotte, J. J., Howard, S. M., Stitt, S., and Dwyer, J. L.: Mapping burned areas using dense time-series of Landsat data, Remote Sens. Environ., 198, 504–522, https://doi.org/10.1016/j.rse.2017.06.027, 2017.

Helman, D.: Land surface phenology: What do we really 'see' from space?, Sci. Total Environ., 618, 665–673, https://doi.org/10.1016/j.scitotenv.2017.07.237, 2018.

Holz, A., Paritsis, J., Mundo, I. A., Veblen, T. T., Kitzberger, T., Williamson, G. J., Aráoz, E., Bustos-Schindler, C., González, M. E., Grau, H. R., and Quezada, J. M.: Southern Annular Mode drives multicentury wildfire activity in southern South America, Proc. Natl. Acad. Sci., 114, 9552–9557, https://doi.org/10.1073/pnas.1705168114, 2017.

Hu, X., Ban, Y., and Nascetti, A.: Uni-Temporal Multispectral Imagery for Burned Area Mapping with Deep Learning, Remote Sens., 13, 1509, https://doi.org/10.3390/rs13081509, 2021.

Huang, C., Thomas, N., Goward, S. N., Masek, J. G., Zhu, Z., Townshend, J. R. G., and Vogelmann, J. E.: Automated masking of cloud and cloud shadow for forest change analysis using Landsat images, Int. J. Remote Sens., 31, 5449–5464, https://doi.org/10.1080/01431160903369642, 2010.

Jolly, W. M., Cochrane, M. A., Freeborn, P. H., Holden, Z. A., Brown, T. J., Williamson, G. J., and Bowman, D. M. J. S.: Climate-induced variations in global wildfire danger from 1979 to 2013, Nat. Commun., 6, https://doi.org/10.1038/ncomms8537, 2015.

Kelly, L. T., Giljohann, K. M., Duane, A., Aquilué, N., Archibald, S., Batllori, E., Bennett, A. F., Buckland, S. T., Canelles, Q., Clarke, M. F., Fortin, M.-J., Hermoso, V., Herrando, S., Keane, R. E., Lake, F. K., McCarthy, M. A., Morán-Ordóñez, A., Parr, C. L., Pausas, J. G., Penman, T. D., Regos, A., Rumpff, L., Santos, J. L., Smith, A. L., Syphard, A. D., Tingley, M. W., and Brotons, L.: Fire and biodiversity in the Anthropocene, Science, 370, eabb0355, https://doi.org/10.1126/science.abb0355, 2020.

Key, C. H. and Benson, N. C.: The Normalized Burn Ratio (NBR): A Landsat TM Radiometric Measure of Burn Severity, Northern Rocky Mountain Science Center, 1999.

King, M. D., Platnick, S., Menzel, W. P., Ackerman, S. A., and Hubanks, P. A.: Spatial and Temporal Distribution of Clouds Observed by MODIS Onboard the Terra and Aqua Satellites, IEEE Trans. Geosci. Remote Sens., 51, 3826–3852, https://doi.org/10.1109/TGRS.2012.2227333, 2013.

Knopp, L., Wieland, M., Rättich, M., and Martinis, S.: A Deep Learning Approach for Burned Area Segmentation with Sentinel-2 Data, Remote Sens., 12, 2422, https://doi.org/10.3390/rs12152422, 2020.

Lentile, L. B., Holden, Z. A., Smith, A. M. S., Falkowski, M. J., Hudak, A. T., Morgan, P., Lewis, S. A., Gessler, P. E., and Benson, N. C.: Remote sensing techniques to assess active fire characteristics and post-fire effects, Int. J. Wildland Fire, 15, 319, https://doi.org/10.1071/WF05097, 2006.

Lizundia-Loiola, J., Franquesa, M., Boettcher, M., Kirches, G., Pettinari, M. L., and Chuvieco, E.: Implementation of the Burned Area Component of the Copernicus Climate Change Service: From MODIS to OLCI Data, Remote Sens., 13, 4295, https://doi.org/10.3390/rs13214295, 2021.

Long, T., Zhang, Z., He, G., Jiao, W., Tang, C., Wu, B., Zhang, X., Wang, G., and Yin, R.: 30 m Resolution Global Annual Burned Area Mapping Based on Landsat Images and Google Earth Engine, Remote Sens., 11, 489, https://doi.org/10.3390/rs11050489, 2019.

McWethy, D. B., Pauchard, A., García, R. A., Holz, A., González, M. E., Veblen, T. T., Stahl, J., and Currey, B.: Landscape drivers of recent fire activity (2001-2017) in south-central Chile, PLOS ONE, 13, e0201195, https://doi.org/10.1371/journal.pone.0201195, 2018a.

McWethy, D. B., Pauchard, A., García, R. A., Holz, A., González, M. E., Veblen, T. T., Stahl, J., and Currey, B.: Landscape drivers of recent fire activity (2001-2017) in south-central Chile, PLOS ONE, 13, e0201195, https://doi.org/10.1371/journal.pone.0201195, 2018b.

Miller, J. D. and Thode, A. E.: Quantifying burn severity in a heterogeneous landscape with a relative version of the delta Normalized Burn Ratio (dNBR), Remote Sens. Environ., 109, 66–80, https://doi.org/10.1016/j.rse.2006.12.006, 2007a.

Miller, J. D. and Thode, A. E.: Quantifying burn severity in a heterogeneous landscape with a relative version of the delta Normalized Burn Ratio (dNBR), Remote Sens. Environ., 109, 66–80, https://doi.org/10.1016/j.rse.2006.12.006, 2007b.

Miranda, A., Altamirano, A., Cayuela, L., Lara, A., and González, M.: Native forest loss in the Chilean biodiversity hotspot: revealing the evidence, Reg. Environ. Change, 17, 285–297, https://doi.org/10.1007/s10113-016-1010-7, 2017.

Moritz, M. A., Batllori, E., Bradstock, R. A., Gill, A. M., Handmer, J., Hessburg, P. F., Leonard, J., McCaffrey, S., Odion, D. C., Schoennagel, T., and Syphard, A. D.: Learning to coexist with wildfire, Nature, 515, 58–66, https://doi.org/10.1038/nature13946, 2014.

Pettorelli, N., Vik, J. O., Mysterud, A., Gaillard, J.-M., Tucker, C. J., and Stenseth, N. Chr.: Using the satellite-derived NDVI to assess ecological responses to environmental change, Trends Ecol. Evol., 20, 503–510, https://doi.org/10.1016/j.tree.2005.05.011, 2005.

Pinto, M. M., Trigo, R. M., Trigo, I. F., and DaCamara, C. C.: A Practical Method for High-Resolution Burned Area Monitoring Using Sentinel-2 and VIIRS, Remote Sens., 13, 1608, https://doi.org/10.3390/rs13091608, 2021.

Radeloff, V. C., Helmers, D. P., Kramer, H. A., Mockrin, M. H., Alexandre, P. M., Bar-Massada, A., Butsic, V., Hawbaker, T. J., Martinuzzi, S., Syphard, A. D., and Stewart, S. I.: Rapid growth of the US wildland-urban interface raises wildfire risk, Proc. Natl. Acad. Sci., 115, 3314–3319, https://doi.org/10.1073/pnas.1718850115, 2018.

Roteta, E., Bastarrika, A., Padilla, M., Storm, T., and Chuvieco, E.: Development of a Sentinel-2 burned area algorithm: Generation of a small fire database for sub-Saharan Africa, Remote Sens. Environ., 222, 1–17, https://doi.org/10.1016/j.rse.2018.12.011, 2019.

Roy, D. P., Ju, J., Mbow, C., Frost, P., and Loveland, T.: Accessing free Landsat data via the Internet: Africa's challenge, Remote Sens. Lett., 1, 111–117, https://doi.org/10.1080/01431160903486693, 2010.

Schroeder, Wilfrid and Giglio, Louis: VIIRS/NPP Thermal Anomalies/Fire Daily L3 Global 1km SIN Grid V001, https://doi.org/10.5067/VIIRS/VNP14A1.001, 2018.

Schroeder, W., Oliva, P., Giglio, L., and Csiszar, I. A.: The New VIIRS 375m active fire detection data product: Algorithm description and initial assessment, Remote Sens. Environ., 143, 85–96, https://doi.org/10.1016/j.rse.2013.12.008, 2014.

Singh, M., Evans, D., Tan, B. S., and Nin, C. S.: Mapping and Characterizing Selected Canopy Tree Species at the Angkor World Heritage Site in Cambodia Using Aerial Data, PLOS ONE, 10, e0121558, https://doi.org/10.1371/journal.pone.0121558, 2015.

Soulard, C., Albano, C., Villarreal, M., and Walker, J.: Continuous 1985–2012 Landsat Monitoring to Assess Fire Effects on Meadows in Yosemite National Park, California, Remote Sens., 8, 371, https://doi.org/10.3390/rs8050371, 2016.

Soverel, N. O., Perrakis, D. D. B., and Coops, N. C.: Estimating burn severity from Landsat dNBR and RdNBR indices across western Canada, Remote Sens. Environ., 114, 1896–1909, https://doi.org/10.1016/j.rse.2010.03.013, 2010.

Stenzel, J. E., Bartowitz, K. J., Hartman, M. D., Lutz, J. A., Kolden, C. A., Smith, A. M. S., Law, B. E., Swanson, M. E., Larson, A. J., Parton, W. J., and Hudiburg, T. W.: Fixing a snag in carbon emissions estimates from wildfires, Glob. Change Biol., 25, 3985–3994, https://doi.org/10.1111/gcb.14716, 2019.

Stillinger, T., Roberts, D. A., Collar, N. M., and Dozier, J.: Cloud Masking for Landsat 8 and MODIS Terra Over Snow-Covered Terrain: Error Analysis and Spectral Similarity Between Snow and Cloud, Water Resour. Res., 55, 6169–6184, https://doi.org/10.1029/2019WR024932, 2019.

Stougiannidou, D., Zafeiriou, E., and Raftoyannis, Y.: Forest Fires in Greece and Their Economic Impacts on Agriculture, KnE Soc. Sci., https://doi.org/10.18502/kss.v4i1.5977, 2020.

Stroppiana, D., Boschetti, M., Zaffaroni, P., and Brivio, P. A.: Analysis and Interpretation of Spectral Indices for Soft Multicriteria Burned-Area Mapping in Mediterranean Regions, IEEE Geosci. Remote Sens. Lett., 6, 499–503, https://doi.org/10.1109/LGRS.2009.2020067, 2009.

Szpakowski, D. M. and Jensen, J. L. R.: A Review of the Applications of Remote Sensing in Fire Ecology, Remote Sens., 11, 2638, https://doi.org/10.3390/rs11222638, 2019.

Úbeda, X. and Sarricolea, P.: Wildfires in Chile: A review, Glob. Planet. Change, 146, 152–161, https://doi.org/10.1016/j.gloplacha.2016.10.004, 2016.

Urrutia-Jalabert, R., González, M. E., González-Reyes, Á., Lara, A., and Garreaud, R.: Climate variability and forest fires in central and south-central Chile, Ecosphere, 9, e02171, https://doi.org/10.1002/ecs2.2171, 2018.

660 Viale, M., Bianchi, E., Cara, L., Ruiz, L. E., Villalba, R., Pitte, P., Masiokas, M., Rivera, J., and Zalazar, L.: Contrasting Climates at Both Sides of the Andes in Argentina and Chile, Front. Environ. Sci., 7, 69, https://doi.org/10.3389/fenvs.2019.00069, 2019.

van Wagtendonk, J. W., Root, R. R., and Key, C. H.: Comparison of AVIRIS and Landsat ETM+ detection capabilities for burn severity, Remote Sens. Environ., 92, 397–408, https://doi.org/10.1016/j.rse.2003.12.015, 2004.

665 Wulder, M. A., White, J. C., Loveland, T. R., Woodcock, C. E., Belward, A. S., Cohen, W. B., Fosnight, E. A., Shaw, J., Masek, J. G., and Roy, D. P.: The global Landsat archive: Status, consolidation, and direction, Remote Sens. Environ., 185, 271–283, https://doi.org/10.1016/j.rse.2015.11.032, 2016.

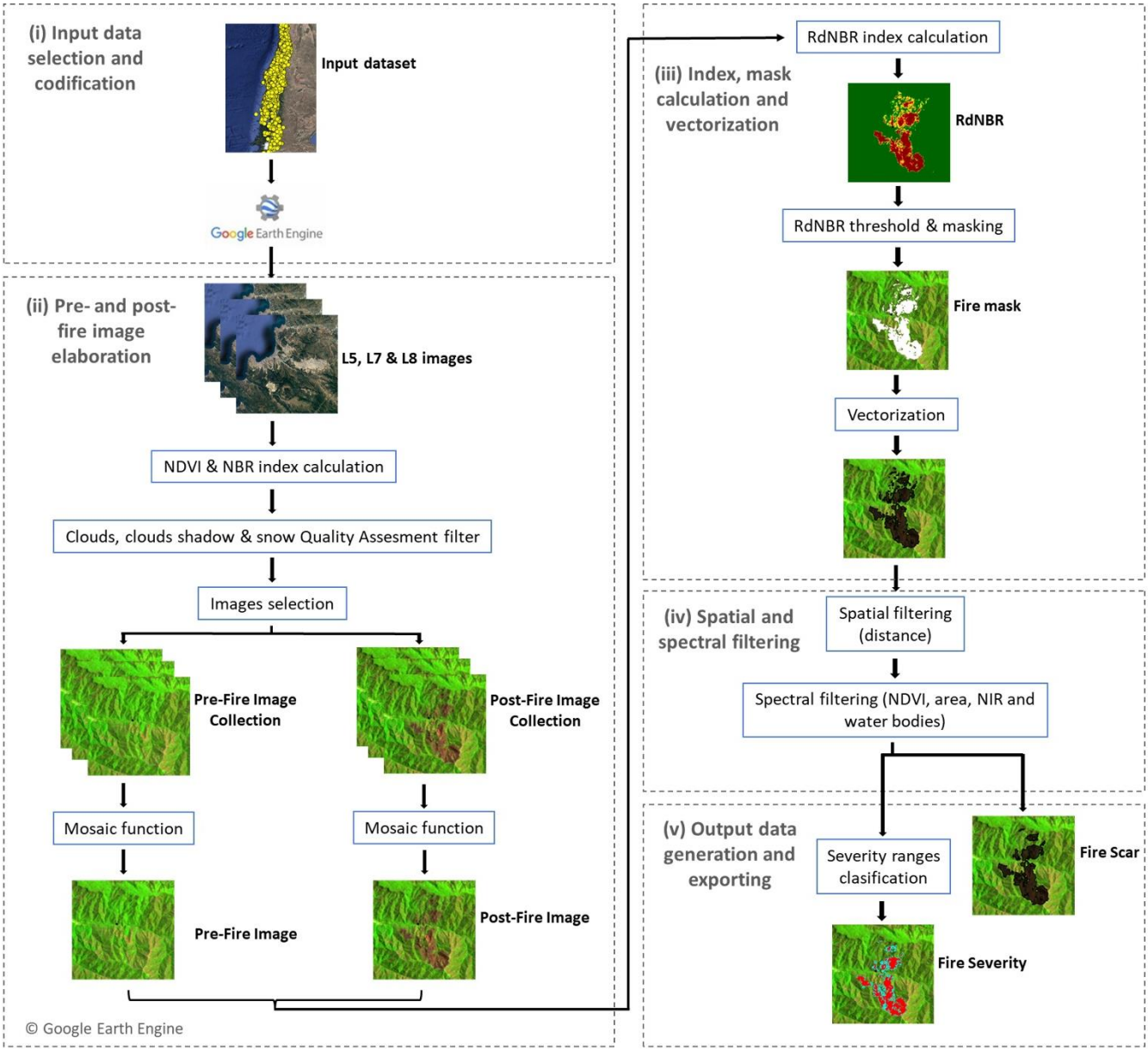

Figure 1: Detailed workflow for individual fire scar generation in Google Earth Engine. See Table 1 for details on NBR and RdNBR.

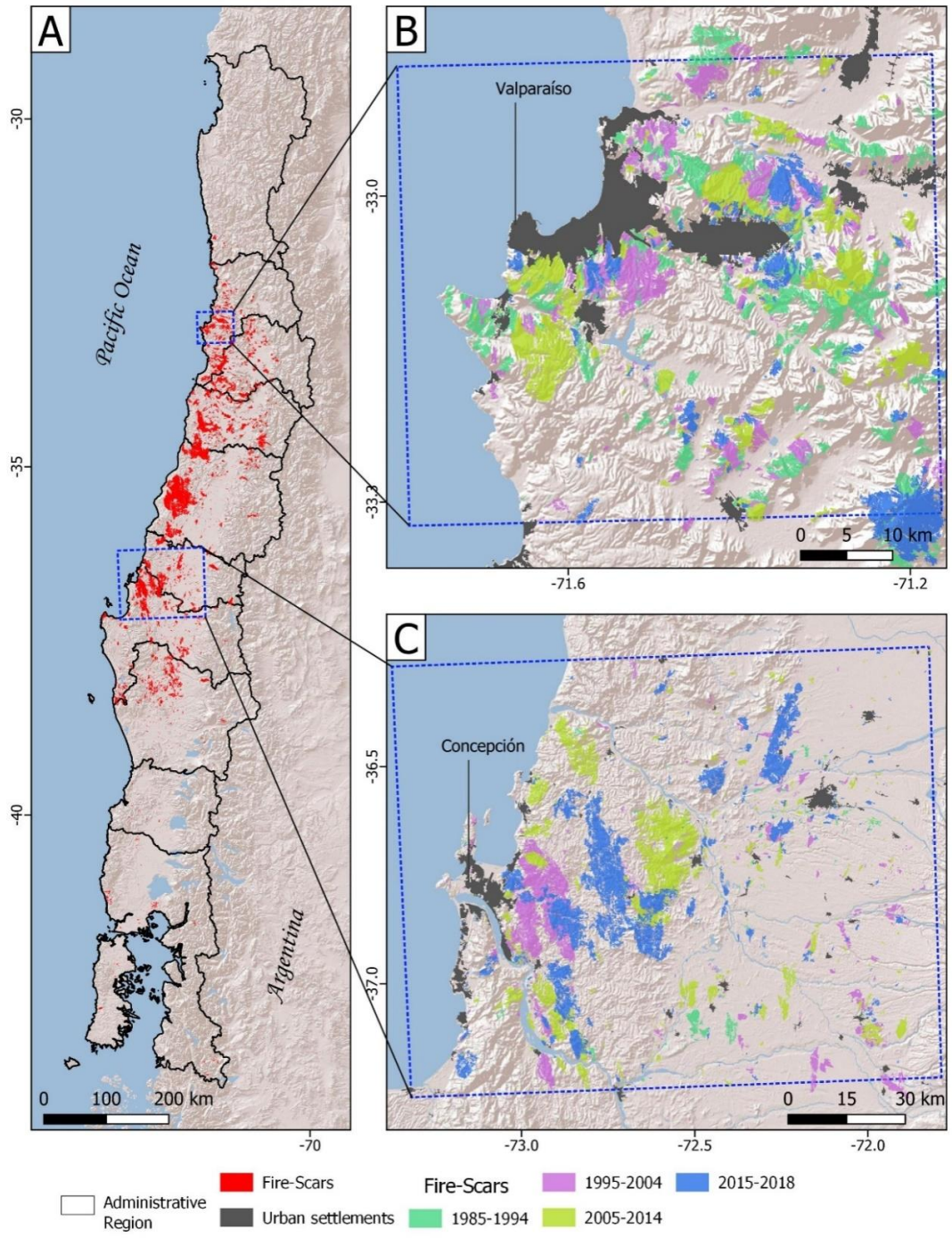

675

Figure 2: A. Geographic distribution of the fire scar database. B and C show examples of fire activity near the cities of Valparaíso and Concepción for different periods.

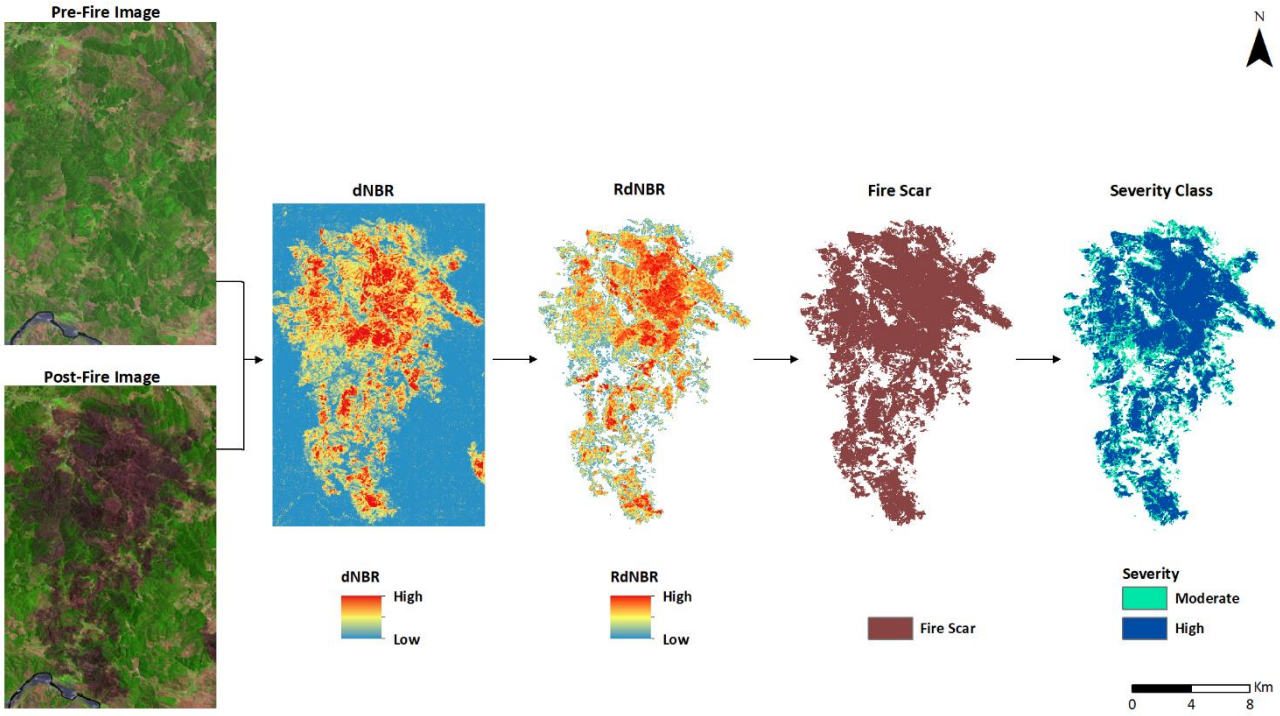

Figure 3: Database content for each reconstructed fire scar. See Table 1 for details on dNBR and RdNBR. Illustrated event is from the Maule region occurred in 2014.

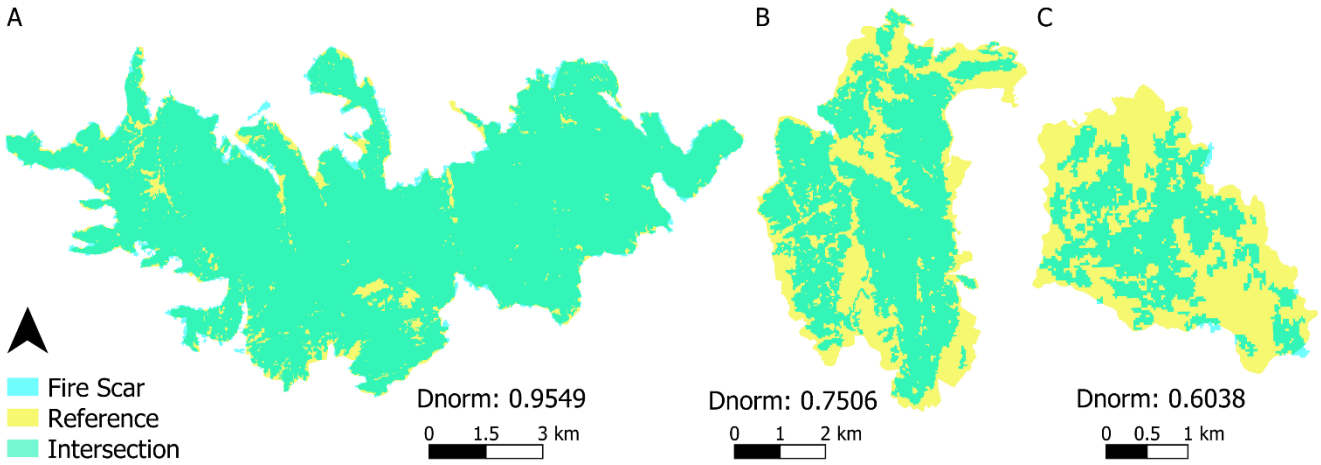

Figure 4: Evaluation of the fire scars. Shown are three examples comparing CONAF's fire scars with the images reconstructed using our Landscape Fire Scars Database methodology. See 2.3 Fire scar evaluation section for detailed description of Dnorm.

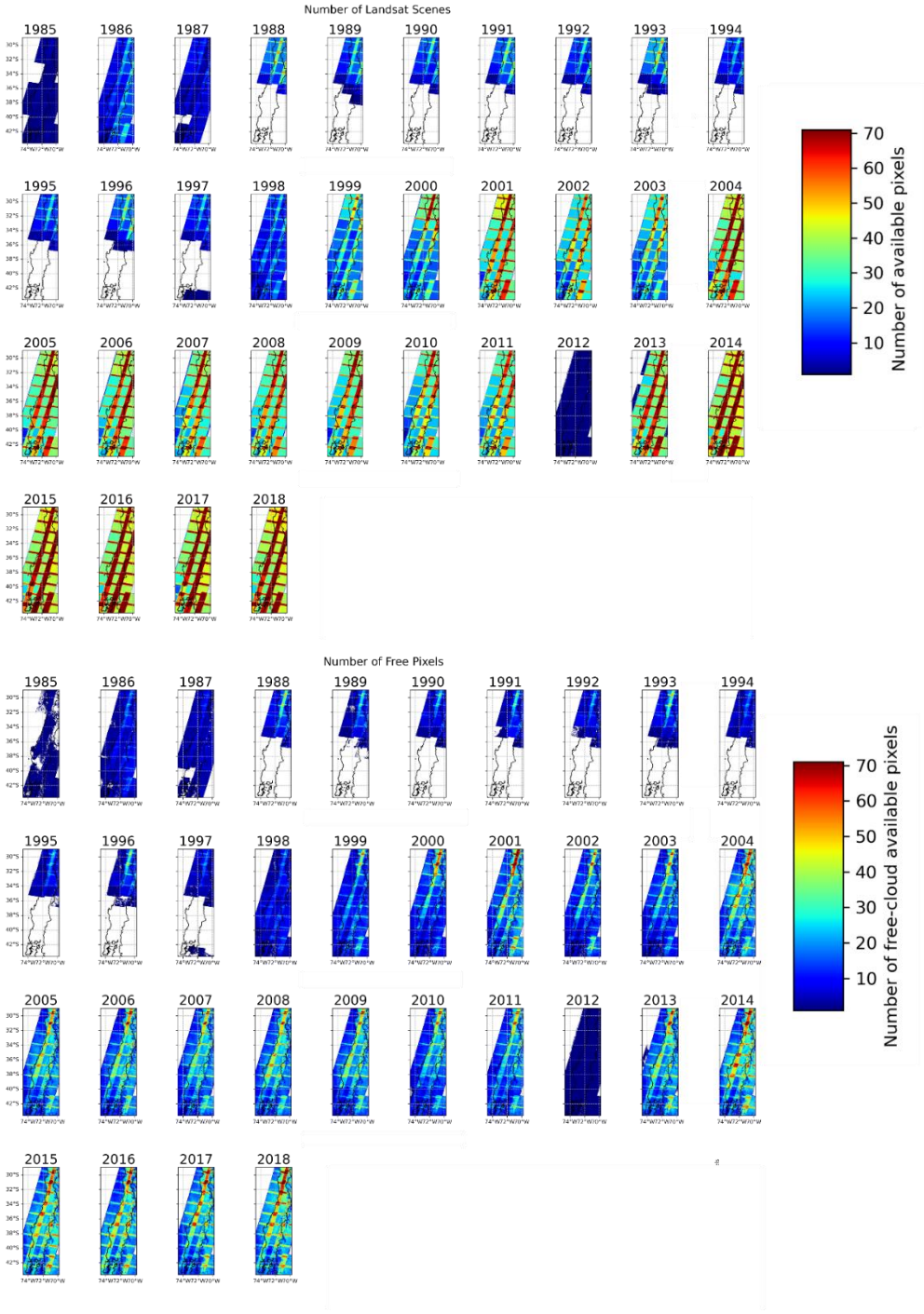

690 Figure 5: Upper panel show available Landsat pixels over study area per each year (1985 – 2018). For the same period, the lower panel represent the number of available Free-Cloud Landsat pixels per year.